https://doi.org/10.1016/j.tws.2020.106722

Net Section Resistance of Bolted S690 Steel Angles Subjected to Tension

Michael CH Yam[a, b], Ke Ke[c, d, *], Binhui Jiang[e], Angus CC Lam[f]

[a] *Department of Building and Real Estate, The Hong Kong Polytechnic University, Hong Kong, China*

[b] *Chinese National Engineering Research Centre for Steel Construction (Hong Kong Branch), The Hong Kong Polytechnic University, Hong Kong, China*

[c] *Key Laboratory of New Technology for Construction of Cities in Mountain Area, School of Civil Engineering, Chongqing University, Chongqing, China*

[d] *Hunan Provincial Key Laboratory for Damage Diagnosis of Engineering Structures, Hunan University, Changsha, China*

[e] *School of Civil Engineering, Central South University, China*

[f] *Department of Civil & Environmental Engineering, University of Macau, Macau SAR, China*

Abstract: Net section rupture is a common failure mode of bolted tension members. In particular, the net section capacity of tension angle is significantly affected by the effect of shear lag. This paper reports the tensile test results of twelve high strength steel angles and six normal steel angles of grade S690 and S275, respectively. The test parameters included steel grades, connection length (bolt number) and out-of-plane eccentricity. All the specimens were failed by net section rupture. Finite element (FE) analysis was used to simulate the structural behaviour of the test specimens and to further interpret the test results. The test and the numerical analysis results showed that the test efficiency of tension angles, which was defined by the ratio of the ultimate test load to the calculated net section resistance, was sensitive to the material ductility and the connection details (i.e. out-of-plane eccentricity and connection lengths). The effectiveness of the available design specifications for quantifying the net section resistance of S690 steel angles was evaluated. A design approach proposed by Yam and colleagues considering the influence of material mechanical characteristics and connection configurations was also revisited. It was found that the current design specifications produced inconsistent predictions of net section resistance of tension angles, whereas the method proposed by Yam and colleagues gave good predictions of net section resistance of bolted S690 steel angles.

Keywords: Shear lag; net section resistance; high strength steel; experiment; finite element model; design method

* Corresponding author. Email address. kerk.ke@outlook.com; keke@hnu.edu.cn

1 Introduction

Tension members made of angles, channels and tees are often used as bracings in steel construction. In a variety of engineering applications, only part of the cross-section of a tension member is connected to the adjacent components via high-strength bolts or welds. A bolted tension angle connected to a gusset plate by one leg is illustrated in Fig. 1. In this context, the connected leg is the one effectively carrying the applied load, whereas the resistance of the outstanding leg may not be effectively mobilised. Hence, the tensile resistance of the section may not be fully developed. This phenomenon is known as "shear lag". Note that the bolt holes may further obstruct the stress flow and produces stress concentration, aggravating the non-uniform tensile stress distribution over the section. The uneven stress distribution is generally most evident near the inner end of the bolt line, and this cross-section is defined as the "critical section", at which fracture tends to occur. Besides, the applied load is transferred along the bolt line which does not coincide with the centroid of the section, and hence produces eccentricity to the connection. The eccentricity would cause a detrimental effect on the net section resistance of the tension member.

The behaviour and net section resistance of tension members have been examined by a number of researchers since the last century [1-4]. For instance, Chesson and Munse [3, 4] examined the behaviour of tension angles based on full-scale experimental programmes and developed an empirical design equation to compute the net section resistance of tension members. Regan and Salter [5] studied the loading carrying behaviour of welded tension angles with various welding configurations, and the authors developed design equations to compute the net section resistance of welded tension angles based on test data

of seventeen welded tension angles. Easterling and Gonzales [6] examined double angles subjected to tension, and the influence of transverse welds on the shear lag was examined. Kulak and Wu [7] studied the tensile resistance of twenty-four single and double bolted tension members and developed novel methods for predicting the resistance of tension angles. Abi-Saad and Bauer [8] proposed an analytical equation for computing the tensile resistance of tension members governed by net section failure. Paula et al. [9] provided sixty-six (66) test data of cold-formed tension angles and developed a test database based on the test programmes from the literature. Prabha et al. [10] put forth a modified design equation for predicting the tensile resistance of cold-formed steel angles failing by net section rupture. Later, Zhu et al. [11] reported more test data of welded single tension angles. Fang et al. [12] studied the behaviour and the tensile resistance of welded tension angles and tees, and the applicability of design specifications for predicting the net section resistance of angles was evaluated. Fleitas et al. [13] examined the net section resistance of bolted cold-formed steel angles using a parametric study. Note that the emphases of the studies mentioned above were generally limited to steel members with nominal yield strength below 460 MPa.

High strength steel (HSS) with a nominal yield strength equal to or over 460 MPa [14-17] has been attracting increasing attention from the academia and engineering community in recent years. Research studies on the mechanical properties of HSS [18-20], HSS connections/components [21-25] and HSS structural systems [26-29] all shed insightful lights on the promise of HSS in steel construction. In engineering practice, the use of HSS may contribute to reducing the size and weight of structures and offer significant savings

in delivery cost and material/energy consumption during steel production. However, HSS generally exhibits lower ductility and a narrower range of post-yielding strain hardening compared to those of normal steel (NS) [19, 20], which may hinder stress redistribution to occur in the vicinity of the critical section of a tension member. Research studies on net section resistance of tension member made of steel with yield strength higher than NS have been conducted by some researchers. Teh and Gilbert [30] examined the net section resistance of steel channels made of cold-reduced sheet with measured yield strength over 530 MPa, and the authors proposed design equations for practical applications. Moze et al. [31] investigated the tension resistance of grade S690 steel plate with holes and the corresponding bolted connections experimentally, and the adequacy of the Eurocode provision for predicting the net section resistance of the connection was revisited. Yam and his co-workers [32] conducted fourteen tensile tests on welded and bolted HSS angles recently. The research findings indicated that HSS material properties (limited ductility and lower tensile strength to yield strength ratio) and connection configurations may reduce the net section efficiency of the bolted angles. However, only seven bolted HSS angles covering two angle sections and one NS specimen were included in [32], which may not fully reveal the load carrying mechanism of bolted HSS angles. In addition, the influence of the connection length and the potential combined effect of this parameter and other influential factors on bolted HSS angles have not been clearly examined. In light of the above, more experimental and analytical work are needed to examine the structural behaviour and net section resistance of bolted HSS tension angles.

The current study includes eighteen (18) tensile tests on bolted steel angles failed by net

103 section rupture. In particular, twelve S690 HSS angles were tested, and for comparison
104 purpose six tests of NS specimens made of grade S275 steel were conducted. The test
105 parameters included steel grade, angle section and bolt arrangement. The new test database
106 covered a wider range of parameters compared to the previous study [32]. The combined
107 effect among material properties and connection details on the net section resistance of the
108 angles, which was not examined in [32], was also studied. Finite element (FE) analysis
109 was employed to simulate the structural behaviour of the angle specimens in order to
110 provide further interpretation of the test observations. The design methods in current codes
111 and a method proposed in [32] were revisited, and their feasibility for quantifying the net
112 section resistance of HSS angles was examined by comparisons against the test results.
113
114 ## 2 Test Programme

115 *2.1 Specimens, test rigs and loading procedure*

116 Eighteen (18) bolted angle specimens were tested. Twelve (12) of them were fabricated
117 using grade S690 steel with a nominal yield stress of 690 MPa, and the remaining six (6)
118 were the NS counterparts made of S275 steel. The steel angles were fabricated using two
119 steel plates through groove welding. The measured thicknesses of the S690 plates were
120 5.94 mm and 7.88 mm on average, and the thickness of S275 steel plates was 5.75 mm.
121 Tension angles were connected to a 10. 41 mm thick gusset plates at each end using Grade
122 12.9 M22 high strength bolts. A typical illustration of a test specimen is shown in Fig. 2.
123 Four angle sections (i.e. 85 × 65 × 6, 65 × 65 × 6, 125 × 65 × 6 and 125 × 65 × 8, unit: mm)
124 were used to study the effects of out-of-plane eccentricities and angle sections. A constant

pitch of 75 mm was designed for all the specimens, whilst the number of bolt was included as one of the test parameters for examining the effect of connection length. The specimen information is summarised in Table 1. The specimen label commences by either 'A' or 'B', representing S275 or S690 steel, respectively. The following number '1', '2', '3' and '4' represents angle section 85 × 65 × 6, 65 × 65 × 6, 125 × 65 × 6 and 125 × 65 × 8 (unit: mm) sections, respectively, and the letter 'S', 'L' or 'E' refers to an angle connected by the short leg, the long leg or the equal leg, respectively. The number of bolts is indicated by the value following 'Bt'. The measured dimensions of specimens are shown in Table 1, and the definitions of the symbols are indicated in Fig. 2.

Tension coupons were extracted from the steel plates and tested according to ASTM A370 [33], and the measured material properties are summarised in Table 2. It is worth noting that although the measured yield strength of 5.94 mm thick S690 steel plate was slightly below the nominal value, the ultimate strain and the ratio of the measured tensile strength to the measured yield strength (f_u/f_y) were typical for S690 steel.

Fig. 3 schematically illustrates the test rig, which was also used in the previous study conducted by Yam and colleagues [32]. In particular, the gusset plates of the specimens were connected to the end fixtures, which were gripped by the crossheads of the testing machine. All the bolted connections were snug tightened by a wrench. The applied loads were obtained by the load cell of the machine, and the elongation of the specimens was recorded by the built-in displacement transducers. Strain gauges with a gauge length of 10 mm were mounted on the specimens to measure longitudinal strain responses at the angle's critical and mid-length section as shown in Fig. 2. In each test, a small preload was used to

147 sit and align the angle specimen and eliminate the slip in the connection. A stroke-control
148 procedure was adopted in the test with the loading rate of 0.2 mm/min exerting tension to
149 the specimen. After the specimens progressing to the inelastic stage, the stroke was
150 maintained for about 90 seconds at various load intervals to allow the specimen to reach
151 static equilibrium, and the corresponding static load values were recorded.
152
153 *2.2 Test results*
154 *2.2.1 Overview*
155 All the specimens were failed by net section rupture at the critical section, and the
156 typical failure modes are shown in Fig. 4. The tensile fracture of angles was initiated from
157 the toe of the connected leg and then propagated to the outstanding leg as shown in the
158 figure. The ultimate load of the specimens and the normalised net section resistance (P_{norm})
159 are shown in Table 1. The normalised net section resistance was determined by dividing
160 the static test ultimate load by $A_n f_u$, where A_n is the measured net-section area of the
161 specimen and f_u is the actual tensile strength of the material. Note that the normalised net
162 section resistance is also known as the test efficiency (i.e. U_{test}). In general, the test
163 efficiency of the grade S275 angle specimens ranged from 0.59 to 1.07, whereas U_{test} of
164 the S690 angle specimens varied from 0.61 to 1.01. It can be seen that the test efficiencies
165 of the specimens were generally lower than unity due to the combined effects of material
166 properties, eccentricity, and connection details. This observation will be further discussed
167 in the following sections.
168 *2.2.2 Load-elongation responses*
169 Fig. 5 gives the normalised load versus elongation curves of all the test specimens. In

general, linear load versus elongation responses were characterised initially, and nonlinear behaviour was observed when the applied load reached approximately 60% to 85% of the ultimate load. Fig. 5 shows that due to the limited deformation capability of S690 material, the normalised load-elongation responses of grade S690 angle specimens generally had a smaller total elongation at the ultimate load compared with those of the S275 counterparts with identical connection configurations. This effect was comparatively more evident in cases with a long connection (e.g. comparison group A2-E-Bt5/B2-E-Bt5 in Fig. 5b and A3-S-Bt5/B3-S-Bt5 in Fig. 5c). Note that the test efficiency of the S275 steel angle A2-E-Bt5 is higher than unity (1.07), and hence the critical section of the angle could develop full net section resistance with adequate strain hardening (f_u/f_y =1.52). This might further allow yielding in the gross section of the angle before fracture of the critical section, and hence contributed to a longer elongation of the member at the ultimate load. In contrast, the lower test efficiency of the S690 steel angle indicated a less effective stress redistribution pattern in the critical section upon reaching the ultimate load due to the limited ductility of S690 steel (ε_u = 0.06, gauge length 50 mm). Thus, yielding of the angle in the gross section might not be effectively developed upon fracture of the critical section, and the corresponding total elongation of the S690 steel angle was reduced.

After reaching the ultimate stage, the applied load deteriorated rapidly as a result of fracture initiation at the critical section. However, all the S275 angles were able to develop pronounced residual resistance in the post-fracture stage, as can be seen from the slight ascending branches in the post-ultimate equilibrium paths (Fig. 5a, Fig. 5b and Fig. 5c). The regained strength and residual ductility could be attributed to the participation of the

192 outstanding leg in carrying the applied load in the post-ultimate stage, recalling that
193 fracture was firstly triggered at the toe area of the connected leg and propagated to the
194 outstanding leg with further elongation (Fig. 4). However, this phenomenon was generally
195 not pronounced for the S690 specimens. These observations imply that the high ductility
196 and evident post-yielding strain hardening of S275 steel was able to effectively mobilise
197 the unconnected leg in carrying the applied load in the post-ultimate stage, and residual
198 strength could be achieved prior to the complete rupture of the section. On the other hand,
199 the less ductile behaviour of S690 steel adversely affected the stress redistribution of the
200 critical section in the post-fracture stage, and complete rupture of the section was triggered
201 before the outstanding leg could be effectively mobilised.

202 *2.2.3 Strain distributions*

203 Fig. 6 presents the representative strain results of the HSS angle specimens (i.e.
204 specimen B1-S-Bt3 and B1-L-Bt5) and the NS counterparts (i.e. specimen A1-S-Bt3 and
205 A1-L-Bt3). Strain readings of critical and mid-length section at representative load levels
206 (i.e. 20%, 40% and 60% of the ultimate load P_{test}) is shown in Fig. 6 to demonstrate the
207 strain evolution of the two sections. The locations of the strain gauges and the theoretical
208 yield strain derived from the actual material properties are also shown in the figure.

209 The general trend of strain distributions of the HSS and NS angle specimens at the
210 critical section is similar, and only the HSS specimens are discussed herein. In particular,
211 at the critical section, the connected leg was generally in tension with tensile yielding
212 firstly triggered near the bolt hole as a result of stress concentration. However, the top edge
213 of the outstanding leg was initially in slight compression due to the combined effects of

214 shear lag and secondary bending according to the strain readings of strain gauge 4. As
215 shown in Fig. 6c, the compressive strains of the short-leg connected specimen B1-S-Bt3
216 kept increasing with increasing applied load. This was because the short-leg connected
217 angle had significant out-of-plane eccentricity, thus causing more evident shear lag and
218 secondary bending. On the contrary, the compression at the top edge of the outstanding leg
219 of specimen B1-L-Bt5 connected by the long leg was mitigated with the applied load
220 increased to 60% of P_{test}, as shown in Fig. 6d. This observation was due to the smaller out-
221 of-plane eccentricity of the long-leg connected angle.

222 At the mid-length section, the material at the top edge of the outstanding leg was
223 initially in compression as a result of secondary bending. As shown in Fig. 6d, specimen
224 B1-L-Bt5 with the largest connection length and the smallest out-of-plane eccentricity
225 reversed the compression at the top edge of the unconnected leg to tension (strain gauge 9)
226 with increasing applied load. On the other hand, the top edge of the outstanding leg of
227 specimen B1-S-Bt3, remained in compression with increasing applied load. Besides, the
228 comparison between the strain responses of S275 and S690 angle specimens (i.e. group
229 A1-S-Bt3/B1-S-Bt3) implied that yielding of the mid-length section of the NS angle might
230 be able to be triggered more readily, as the strain of the section was closer to the yield
231 strain at 60% of P_{test}, echoing the larger total elongation of S275 angles shown in Fig. 5.
232 More evidence substantiating this argument will be provided in later sections based on
233 finite element analysis of the angle specimens.

234

3 Discussions of test and finite element analysis results

3.1. Discussions of test results

3.1.1 Effects of type of steel

The test results showed that the limited ductility of HSS steel material adversely affected the load carrying behaviour of bolted tension angles which echoed the test observations from [32]. According to Table 1, the test efficiencies of S690 angle specimens are generally lower than those of the S275 counterparts with identical section and connection configuration. The reduction in test efficiency varied from 8% to 17%. However, the comparison group A1-S-Bt3/B1-S-Bt3 and A3-S-Bt3/B3-S-Bt3 are exceptions with the test efficiency of the S690 angle equal to or even slightly higher than that of the S275 specimens. Note that in these cases the angles generally had a significant out-of-plane eccentricity (i.e. a considerable outstanding leg length) and a short connection (i.e. three bolts). In this scenario, the influence of the connection configurations dominated the tensile behaviour of the angle specimens. The angles failed to mobilise effectively the outstanding leg in carrying the applied load. However, the influence of steel grades became more pronounced in cases with long-leg connected angles and long connections. In particular, the test efficiency of a long-leg connected S690 angle specimen B1-L-Bt3 (0.85) was lower than that of the S275 counterpart specimen A1-L-Bt3 (0.92). The test efficiency of specimen B3-S-Bt5 and A3-S-Bt5 with a long connection are 0.69 and 0.83, respectively. This phenomenon was due to the fact that the shear lag effect was reduced by a long-leg connected angle and a long connection, and therefore the effect of material ductility on the tensile behaviour and strength of the angle specimens became more

257 pronounced. Since the limited material ductility of S690 steel material might not allow
258 sufficient stress redistribution to occur in mobilising the outstanding leg prior to failure,
259 the test efficiency of the HSS angle was reduced.

260 *3.1.2 Effects of out-of-plane eccentricity*

261 The test results confirmed that the test efficiency decreases with increasing out-of-plane
262 eccentricity for both S690 and S275 angle specimens. In particular, the S690 angle
263 specimen B1-L-Bt3 connected by the long leg achieved a test efficiency of 0.85, whereas
264 the short-leg connected counterpart (i.e. B1-S-Bt3) with a more significant out-of-plane
265 eccentricity achieved a lower efficiency of 0.74. Similarly, specimens B1-L-Bt5 and B1-S-
266 Bt5 produced the test efficiency of 1.01 and 092, respectively. The adverse effect of
267 increasing out-of-plane eccentricity can also be seen according to the test efficiency of the
268 comparison group B3-S-Bt5/B2-E-Bt5 with the identical connected leg and varied
269 outstanding legs, and the test efficiency of specimen B3-S-Bt5 (outstanding leg 125 mm)
270 is 30% lower than that of specimen B2-E-Bt5 (outstanding leg 65 mm). Similar
271 observations were characterised for the S275 angle specimens. In general, these expected
272 findings are consistent with those characterised from previous research works [3, 4, 9, 32].
273

274 *3.1.3 Effects of connection length*

275 The test data showed that the test efficiency of the specimens generally increases with
276 increasing connection length. Specifically, two equal-leg connected S690 angle specimens
277 B2-E-Bt3 (connection length 100 mm) and B2-E-Bt5 (connection length 200 mm)
278 achieved the test efficiency of 0.80 and 0.98, respectively, which represents an increase of
279 23% in test efficiency with connection length increased by 100%. Similarly, the test

efficiencies of S275 angle specimens A2-E-Bt3 and A2-E-Bt5 are 0.88 and 1.07, respectively, and the corresponding increase of the test efficiency is 22%. However, the effect of connection length on the test efficiency was relatively less evident in case of short-leg connected S690 steel angles. The test efficiency of specimens B3-S-Bt3, B3-S-Bt4 and B3-S-Bt5 are 0.61, 0.69 and 0.69, respectively, representing an increase of only 13% in test efficiency with an increase in connection length of 100%. Similar findings were recorded for specimens B4-S-Bt3, B4-S-Bt4 and B4-S-Bt5. Therefore, it can be seen that a short-leg connected S690 angle, which has lower material ductility and a higher out-of-plane eccentricity, may further prohibit the effective mobilisation of the outstanding leg to resist the applied load. Thus, the beneficial effect of an increasing connection length in enhancing the net section resistance was not pronounced.

3.2 Finite element analysis

3.2.1 Modelling techniques

To facilitate further interpretation of the test results, finite element (FE) models of the specimens were developed using ABAQUS [34]. A typical FE model of the angle specimen is presented in Fig. 7. Eight-node solid elements (i.e. C3D8R) were used to model the steel angle, bolts and gusset plates. Four elements were developed in the thickness direction for all the components to avoid the "hourglass" [34] effect. A "general contact" method was employed to simulate the interaction among the components. The "hard contact" and "penalty friction" algorithm were adopted to reproduce the contact behaviour, whereas the influence of the bolt clamping force was ignored. This simplification is reasonable since snug tight condition by hand wrench was used to install

the bolts. To simulate the constraint by the end fixtures in the tests, all the degrees of freedom in the connection region of the gusset plate were coupled using "kinematic coupling", whereas translational displacement along the angle elongation direction was allowed (U3 in Fig. 7). To model the minor elastic elongation of the test assembly during loading, elastic springs elements in the U3 direction were introduced, and a consistent stiffness was calibrated based on the initial slope of the load versus elongation responses of the specimens. "Dynamic/explicit" solver of ABAQUS was utilised to avoid convergence issues in the post-ultimate stage.

An isotropic plastic model with von Mises yield criterion was used. True stress-strain responses derived from the nominal stress-strain curves obtained from the coupon results were adopted in the modelling. Specifically, the true stress-strain relationship before necking can be expressed by the following equation.

$$\sigma_t = \sigma_{no}(1 + \varepsilon_n) \tag{1}$$

$$\varepsilon_t^p = \ln(1 + \varepsilon_n) - \frac{\sigma_t}{E} \tag{2}$$

where σ_t = true stress, σ_{no} = nominal stress (engineering stress), ε_t^p = true plastic strain, ε_n = nominal strain (engineering strain) and E = the elastic modulus. Recognising that the above correlations were valid only before necking, approximations were needed to determine the true stress-strain relationship in the post-necking branch. A trial-and-error procedure was adopted by assuming that the true stress-strain curve remains linear [35, 36] after necking. The rationale of using a trial-and-error process in simulating the post-necking behaviour of the material are supported by recent research works. The "Damage for Ductile Metals" module [34] was implemented to simulate damage evolution and

fracture of the material. The "fracture strain" and "damage evolution index" in the module quantify the strain corresponding to cracking inception and the deterioration rate of the material, respectively. To account for the influence of complex stress state on the fracture of tension angles, the classical Johnson-Cook damage function [37] was used to develop the relationship between the fracture strain (ε_f) and stress triaxiality (η) based on iterations, i.e. $\varepsilon_f = a + be^{-c\eta}$, where a, b and c are coefficients to be calibrated. Based on the available test data, a=0.063, b=0.094 and c=2.800 were finalised for S275 steel. For S690 steel, a=0.040, b=0.800 and c=2.500 were used. Since the net section resistance of all the specimens was dominated by tensile failure of the material near the bolt hole, the adopted fracture model excluding the influence of lode angle [38-40], which quantifies the influence of the shear action on the fracture behaviour, is reasonable. To determine the damage-evolution index, a linear method was assumed to simulate the material deterioration until complete stiffness loss. As the mesh property would affect the fracture prediction significantly, a refined mesh was used in the bolted connection area of the FE models where fracture was expected to occur. An element size of 2.0 mm approximately was finalised using a mesh sensitivity analysis. More information about the rationale of the adopted fracture simulation strategy in ABAQUS can be found in [34], and the adequacy and limitation of the methods was also recorded in the literature [41-45].

3.2.2 FE results and further discussions

The test-to-FE ratios computed by the ratio of the ultimate strength of the specimens (P_{test}) to the FE prediction (P_{FE}) are shown in Table 1. The test-to-FE ratio of S690 angle specimens ranged from 1.01 to 1.12, with an average P_{test}/P_{FE} ratio of 1.06 and a

346 coefficient of variation (CoV) of 0.041. The test-to-FE ratio of S275 angles varied from
347 1.02 to 1.18, with an average P_{test}/P_{FE} ratio of 1.09 and a CoV of 0.065. The applied load-
348 elongation responses of typical specimen groups (A1-S-Bt3, A1-L-Bt3, A3-S-Bt3, A3-S-
349 Bt5, B1-S-Bt3, B1-L-Bt3, B3-S-Bt3, B3-S-Bt5, B4-S-Bt3 and B4-S-Bt5) covering varied
350 steel grades, out-of-plane eccentricities and connection lengths were compared with the
351 corresponding FE results, as shown in Fig. 8. In general, good correlation between the
352 load-deflection responses by tests and FE predictions is observed. The strain readings at
353 the critical and the mid-length sections corresponding to 20%, 40% and 60% of the
354 ultimate load were extracted from the FE models and plotted against the test results as
355 shown in Fig. 6, which substantiated the validity of the FE models. In addition, the strain
356 responses at the mid-length section corresponding to 95% of the ultimate load were
357 extracted from the FE results and shown in Fig. 6. It can be seen that the S275 angles
358 could generally develop yielding in the mid-length section when the applied load
359 approached the ultimate, whereas this phenomenon was not evident for the S690 angles.
360 This finding echoes the generally larger total elongation of S275 specimens as observed
361 from the test results. Note that the damage evolution from necking to fracture obtained
362 from the FE predictions are also included in Fig. 8 for a clearer interpretation of the
363 structural behaviour of the specimens. The failure of the critical section was triggered by
364 necking of the toe of the connected leg identified as “1” in the figure. Fracture of the
365 material near the bolt hole occurred upon further loading identified as “2” in the figure.
366 The failure modes of the test specimens compared well with those of the FE results as
367 shown in Fig. 8.

368 To offer an in-depth understanding of the stress evolution, the normal stress at various
369 loading levels (i.e. 10%, 20%, 50%, 70% and 100% of P_{FE}) from the FE results of
370 specimen B3-S-Bt5 (S690) and specimen A3-S-Bt5 (S275) at the critical sections were
371 examined as shown in Fig. 9. The figure shows the normal stress evolution at the
372 connected leg and the outstanding leg, and the positive and negative values represent
373 tensile and compressive stress, respectively. Non-uniform normal stress distribution was
374 evident in the initial loading stages (i.e. 10% and 20% of P_{FE}) along the tensile plane of the
375 connected leg (i.e. path "X2" in Fig. 9), and the maximum stress was seen at the edge of
376 the bolt hole due to stress concentration. With further increase of the applied load, the
377 angle progressed into the inelastic stage, and stress redistribution occurred across the
378 critical section of the connected leg. At the ultimate stage, the normal stress across the
379 critical section of the connected leg approached uniform irrespective of the steel grade as
380 indicated by the tensile stress distribution along path "X2" in Fig. 9. On the other hand,
381 linear normal stress distribution was characterised for the outstanding leg (i.e. path "X1" in
382 Fig. 9) of both angles initially, and the top portion of the leg was in slight compression,
383 echoing the strain readings from the test results. Subsequently, the normal stress
384 distribution along path "X1" became nonlinear with increasing applied load. At the
385 ultimate stage, the compressive stress in the outer edge of the outstanding leg was
386 increased significantly due to the significant secondary bending effect, which was
387 consistent with test observations. However, it should be noted that at the ultimate stage the
388 compression area of the outstanding leg of the S275 specimen (A3-S-Bt5) was reduced
389 almost by half whereas the corresponding compression area of the S690 specimen (B3-S-

Bt5) remained almost unchanged. This demonstrated that the limited ductility of S690 steel material did not allow sufficient deformation of the specimen to occur prior to reaching the ultimate load, and therefore prohibited the effective mobilisation of the outstanding leg to resist the applied load. These observations echoed the test result that specimen B3-S-Bt5 achieved a much lower test efficiency compared with that of A3-S-Bt5. Based on the test and the FE results, it can be seen that the limited ductility of HSS lessens the effectiveness of stress redistribution across the critical section of S690 angle specimens, and hence reduces the test efficiency.

4 Design comments

The adequacy of the design equations in major specifications CSA S16-14 [46], AS 4100 [47], Eurocode 3 [48] and AISC 360-16 [49] for predicting the net section resistance of single bolted tension angle specimens is examined in this section. The design equations documented in the specifications mentioned above are reproduced in Table 3. Although various design specifications employ different equations, they were developed based on a similar framework by considering strength reductions based on the net area of the angles.

The test-to-predicted ratios by the above design equations are summarised in Table 4. The actual material properties were used to compute the predicted resistance. Resistance factors, capacity factors and partial safety factors accounting for reliability were taken as unity. The test results of seven S690 angle specimens in [32] were also included in the discussion to enlarge the test results database. CSA S16-14 [46] produced an average test-to-predicted ratio of 1.06 with a CoV of 0.175 and an average test-to-predicted ratio of

412 1.27 with a CoV of 0.173 for the S690 angle specimens and the S275 angle specimens,
413 respectively. Similarly, AS 4100 [47] produced generally conservative predictions of the
414 net section resistance for both S275 and S690 angle specimens, whereas the conservatism
415 of the predictions was reduced in case of S690 specimens. Eurocode 3 [48] produced an
416 average test-to-predicted ratio of 1.78 with a CoV of 0.087 for the S690 angle specimens,
417 and an average test-to-predicted ratio of 1.79 accompanied with a CoV of 0.154 for the
418 S275 angle specimens, showing the overly conservative nature of the method. The average
419 test-to-predicted ratio predicted by the AISC 360-16 [49] design equations was 0.90 with a
420 CoV of 0.100 for the S690 angle specimens. Comparatively, the average test-to-predicted
421 ratio of 0.98 with the CoV of 0.108 were obtained for S275 angle specimens.

422 Based on the available test data, it can be seen that the design equations in the
423 specifications produced inconsistent predictions of the net section resistance of the angle
424 specimens, and unsafe predictions were more obvious in cases of S690 steel angles.
425 Although the average test-to-predicted ratio for the S690 angle specimens by the equations
426 in CSA S16-14 [46] was on the conservative side, significantly unsafe predictions were
427 recorded for some S690 specimens according to Table 4 (e.g. B4-S-Bt4 with the test-to-
428 predicted ratio of 0.79). Also, the generally unconservative predictions by AISC 360-16
429 [49] in cases of S690 steel indicated that the design method may not be applicable to HSS
430 angles. These findings might be attributed to the fact that the influence of material property
431 of S690 steel (i.e. f_u/f_y =1.04~1.12 and ε_u = 0.06 with a gauge length of 50 mm) was not
432 taken into account by the design equations. As revealed by the test results and the stress
433 evolution behaviour in the FE study (Fig. 9), the outstanding leg of the S690 steel angles

may not be effectively mobilised to resist tension prior to reaching the ultimate load, and thus the above design equations developed based on normal steels are prone to overestimating the net section resistance of S690 steel angles. This could be further confirmed from the unsafe predictions by CSA S16-14 [46] and AISC 360-16 [49] in cases of S690 steel angles with a considerable outstanding leg length (e.g. B3 series and B4 series angles), in which case stress redistribution to the outstanding leg might not be effective.

Yam and his co-workers [32] developed a modified design method based on a numerical study to evaluate the net section resistance of HSS tension angles. The method considers the combined effect of the f_u/f_y ratio of the material and the configuration of the connections. In particular, the net section resistance of a single tension angle is computed by the following

$$P_{\mathrm{Yam}} = \beta_{\mathrm{m}}\beta_t\left(1-\frac{\overline{x}}{l}\right)A_{\mathrm{n}}f_{\mathrm{u}} \tag{3}$$

$$\beta_{\mathrm{m}} = -0.34\omega^{-1} + 1.14 \tag{4}$$

$$\beta_t = 0.4\,S/S' + 0.7 \tag{5}$$

where ω = ultimate strength to the yield strength ratio of the material, S = connected leg length and S'= outstanding leg length. The definition of A_{n}, f_{u}, $\overline{x}$, and l are identical to those specified in Table 3, and the predictions by the method is summarised in Table 4. Employing the Yam's equation [32], an average test-to-predicted ratio of 1.06 with a CoV of 0.065 was recorded for S690 steel angles, and an average test-to-predicted ratio of 1.03 with a CoV of 0.095 was obtained for the S275 steel specimens. As can be seen, the equations proposed by Yam and co-workers [32] provided good estimates of the net

456 section resistances of both S275 and S690 steel angles. Based on the available test results,
457 it is recommended that the equation proposed by Yam and co-workers to be applied to
458 quantifying the net section resistance of bolted S690 HSS angles. However, caution should
459 be exercised when using the Yam's equation outside the range of parameters discussed in
460 [32] and the current study. Reliability analyses are also expected to develop a full-fledged
461 design guideline for practical applications.
462
463
464 **5 Conclusions**

465 A full-scale test programme on the net section resistance of S690 high strength steel
466 (HSS) bolted angles is reported in this study. Eighteen tests on single bolted tension angles
467 were conducted, of which twelve specimens were S690 steel angles and the remaining six
468 were S275 steel counterparts. The test parameters included steel grade, out-of-plane
469 eccentricity and connection length (i.e. bolt number). The test matrix covered a broadened
470 range of parameters compared with a previous study [32], and the comparative study
471 between the behaviour of S690 and S275 bolted angles was conducted. The test results
472 showed that the behaviour and failure modes of S690 HSS tension angles were similar to
473 those made of normal steel (i.e. S275 steel) angles. The combined effect of material
474 characteristics and connection configurations on the net section resistance of tension
475 angles was also observed. In general, the test efficiency decreased with higher steel grade,
476 and this trend was more obvious in cases of angles with a long-leg connection and long
477 connection length. As expected, the test efficiency decreased with increasing out-of-plane

478 eccentricity for both S690 and S275 steel angles. In addition, the test efficiency of S690
479 and S275 steel angles generally increased with connection length, but this trend was not
480 pronounced for S690 steel angles connected by the short leg.

481 To help interpret the test results, finite element (FE) models of the specimens were
482 developed. In general, the FE predictions agreed well with the test responses, and the
483 behaviour of tension angles from yielding inception to failure was well reproduced by the
484 FE models. The normal stress evolution process at the critical sections of angles from the
485 initial loading stage to the ultimate load, which could not be captured in the test, were
486 further examined using the validated FE models. The results confirmed that the
487 outstanding leg of the S690 steel angle might not be fully mobilised to carry the applied
488 load prior to failure of the net section, and the reduced ductility of S690 steel would
489 appreciably affect the net section resistance of bolted tension angles. These results echoed
490 the test observations that the test efficiency of the S690 angle specimens was generally
491 lower than that of the S275 angle specimens with identical connection configurations.

492 The test results were compared to the predictions by the design equations documented in
493 major design specifications and to those by the equation proposed by the authors and
494 colleagues [32]. It was observed that the design equations in CSA S16-14 [46] and AISC
495 360-16 [49] produced unconservative estimates of the net section resistance for S690 steel
496 angles, particularly in cases of short-leg connected angles with a considerable outstanding
497 leg length. AS 4100 [47] produced conservative predictions of the net section resistance
498 for S275 and S690 steel angles, however, the coefficients of variation of the test-to-
499 predicted ratios were significant. Eurocode 3 [48] led to overly conservative predictions of

500 the net section resistance of both S275 and S690 steel angles. The inconsistent predictions
501 by the codified equations may be explained by the fact that these design methods do not
502 consider the effect of material property on the net section resistance of tension members.
503 In contrast, the design equation proposed by the authors and colleagues [32] accounting for
504 the combined effect of f_u/f_y ratio and connection configurations produced good estimates of
505 the net section resistance of both S275 and S690 angle specimens. Therefore, it is
506 recommended to use the equation in [32] to predict the net section resistance of bolted
507 S690 HSS angles. However, caution should be exercised when using the equation outside
508 the range of parameters discussed in [32] and the current study.
509
510 **Acknowledgement**

511 This work is supported by the Research Grants Council of the Hong Kong Special
512 Administrative Region, China with Grant No. PolyU 152650/16E. The corresponding
513 author would like to thank the National Natural Science Foundation of China (Grant No.
514 51890902 and 51708197) for providing partial supports.
515
516 **References**

517 [1] Davis RP, Boomsliter GP. Tensile tests of welded and riveted structural members. J
518 Am Weld Soc 1934; 13(4): 21-27.
519 [2] Gibson G, Wake B. An investigation of welded connections for angle tension members.
520 Weld J 1942; 21(1): 44-49.
521 [3] Chesson E, Munse WH. Riveted and bolted joints: Truss-type tensile connections. J

522 Struct Div, 1963; 89(1): 67-106.
523 [4] Munse WH, Chesson E. Riveted and bolted joints: net section design. J Struct Eng
524 1963; 89(1): 107-126.
525 [5] Regan P, Salter P. Tests on welded-angle tension members. Struct Eng 1984; 62: 25-30.
526 [6] Easterling WS, Gonzales L. Shear lag effects in steel tension members. Eng J 1993; 3:
527 77-89.
528 [7] Kulak GL, Wu EY. Shear lag in bolted angle tension members. J Struct Eng 1997;
529 123(9): 1144-1152.
530 [8] Abi-Saad G, Bauer D. Analytical approach for shear lag in welded tension members.
531 Can J Civil Eng 2006; 33: 384-94.
532 [9] Paula VFD, Bezerra LM, Matias WT. Efficiency reduction due to shear lag on bolted
533 cold-formed steel angles. J Constr Steel Res 2008; 64(5): 571-583.
534 [10] Prabha P, Jayachandran SA , Saravanan M , Marimuthu V. Prediction of the tensile
535 capacity of cold formed angles experiencing shear lag. Thin Wall Struct 2011;
536 49(11):1348-1358.
537 [11] Zhu HT, Yam MCH, Lam ACC, Iu VP. The shear lag effects on welded steel single
538 angle tension members. J Constr Steel Res 2009; 65:1171-1186.
539 [12] Fang C, Lam ACC, Yam, MCH. Influence of shear lag on ultimate tensile capacity of
540 angles and tees. J Constr Steel Res 2013; 84: 49-61.
541 [13] Fleitas I, Bonilla J, Bezerra LM, Mirambell E, Net section resistance in bolted cold-
542 formed steel angles under tension. J Constr Steel Res 2020: 105841. (In press)
543 [14] Ricles JM, Sause R, Green PS. High-strength steel: implications of material and
544 geometric characteristics on inelastic flexural behavior. Eng Struct 1998; 20(4):323-

335.

[15] Bjorhovde R. Development and use of high performance steel. J Constr Steel Res 2004; 60(3-5):393-400.

[16] Aslani F, Uy B, Tao Z, Mashiri FR. Behaviour and design of composite columns incorporating compact high-strength steel plates. J Constr Steel Res 2015; 107: 94-110.

[17] Huang ZC, Li DX, Uy B, Thai HT, Hou C. Local and post-local buckling of fabricated high-strength steel and composite columns. J Constr Steel Res 2019; 154: 235-249.

[18] Wang YB, Lyu YF, Wang YZ, Li GQ, Liew JYR. A reexamination of high strength steel yield criterion. Constr Build Mater 2020; 230: 116945.

[19] Hu F, Shi G. Constitutive model for full-range cyclic behavior of high strength steels without yield plateau. Constr Build Mater 2018; 162:596-607.

[20] Ho HC, Liu X, Chung KF, Elghazouli AY, Xiao M. Hysteretic behaviour of high strength S690 steel materials under low cycle high strain tests. Eng Struct 2018; 165: 222-236.

[21] Wang YB , Li GQ , Cui W , Chen SW. Seismic behavior of high strength steel welded beam-column members. J Constr Steel Res 2014; 102:245–255.

[22] Lan X, Chan TM, Young B. Structural behaviour and design of chord plastification in high strength steel CHS X-joints. Constr Build Mater 2018; 191: 1252-1267.

[23] Pucinotti R, Tondini N, Zanon G, Bursi OS. Tests and model calibration of high-strength steel tubular beam-to-column and column-base composite joints for moment-resisting structures. Earthq Eng Struct Dyn 2015; 44(9):1471–1493.

[24] Liu X, Chung KF. Experimental and numerical investigation into temperature histories and residual stress distributions of high strength steel S690 welded H-sections. Eng Struct 2018; 165:396-411.

570 [25] Chung K, Ho H, Hu Y, Wang K, Liu X, Xiao M, Nethercot D. Experimental evidence
571 on structural adequacy of high strength S690 steel welded joints with different heat
572 input energy. Eng Struct 2020; 204: 110051.
573 [26] Hu F, Shi G, Shi Y. Experimental study on seismic behavior of high strength steel
574 frames: Global response. Eng Struct 2017; 131:163–179.
575 [27] Chen YY, Ke K. Seismic performance of high-strength-steel frame equipped with
576 sacrificial beams of non-compact sections in energy dissipation bays. Thin Wall Struct
577 2019; 139: 169-185.
578 [28] Tian XH, Su MZ, Lian M, Wang F and Li S. Seismic behavior of K-shaped
579 eccentrically braced frames with high-strength steel: shaking table testing and FEM
580 analysis. J Constr Steel Res 2018; 143: 250-263.
581 [29] Ke K, Wang W, Yam MCH, Deng L. Residual displacement ratio demand of
582 oscillators representing HSSF-EDBs subjected to near-fault earthquake ground
583 motions. Eng Struct 2019; 191:598-610.
584 [30] Teh LH, Gilbert BP. Net section tension capacity of cold-reduced sheet steel channel
585 braces bolted at the web. J Struct Eng 2012; 139(5): 740-747.
586 [31] Može P, Beg D, Lopatič J. Net cross-section design resistance and local ductility of
587 elements made of high strength steel. J Constr Steel Res 2007; 63(11): 1431-1441.
588 [32] Ke K, Xiong YH, Yam MCH, Lam ACC, Chung KF. Shear lag effect on ultimate
589 tensile capacity of high strength steel angles. J Constr Steel Res 2018; 145: 300-314.
590 [33] ASTMA370, Standard test methods and definitions for mechanical testing of steel
591 products, American Society for Testing and Material, Philadelphia, PA, 2002.
592 [34] ABAQUS Analysis User's Manual. ABAQUS Standard, Version 6.12; 2012.
593 [35] Jia LJ, Kuwamura H. Ductile fracture simulation of structural steels under monotonic
594 tension. J Struct Eng 2013; 140(5): 04013115.

595 [36] Liao FF, Wang W, Chen YY. Ductile fracture prediction for welded steel connections
596 under monotonic loading based on micromechanical fracture criteria. Eng Struct 2015;
597 94: 16-28.
598 [37] Johnson GR, Cook WH. Fracture characteristics of three metals subjected to various
599 strains, strain rates, temperatures and pressures. Engng Fract Mech 1985; 21: 31-48.
600 [38] Ma X, Wang W, Chen YY, Qian XD. Simulation of ductile fracture in welded tubular
601 connections using a simplified damage plasticity model considering the effect of stress
602 triaxiality and Lode angle. J Constr Steel Res 2015; 114: 217-236.
603 [39] Xu F, Chen J, Chan TM. Numerical analysis and punching shear fracture based design
604 of longitudinal plate to concrete-filled CHS connections. Constr Build Mater 2017; 156:
605 91-106.
606 [40] Wang J, Wang W, Qian X. Progressive collapse simulation of the steel-concrete
607 composite floor system considering ductile fracture of steel. Eng Struct 2019; 200:
608 109701.
609 [41] Li L, Wang W, Chen YY, Lu Y. Effect of beam web bolt arrangement on catenary
610 behaviour of moment connections. J Constr Steel Res 2015; 104: 22-36.
611 [42] Sadek F, Main JA, Lew HS, Bao YH. Testing and analysis of steel and concrete
612 beam-column assemblies under a column removal scenario. J Struct Eng 2011; 137(9):
613 881-892.
614 [43] Yang B, Tan KH. Numerical analyses of steel beam-column joints subjected to
615 catenary action. J Constr Steel Res 2012; 70(70): 1-11.
616 [44] Samimi MJ, Marnani JA, Otaghsaraie SMS, Otaghsaraie SRS. Block shear
617 experimental and numerical studies on hot rolled channel and gusset plate with
618 staggered bolted connection. Thin Wall Struct 2016; 108:153-162.
619 [45] Fang C, Lam ACC, Yam MCH, Seak KS. Block shear strength of coped beams with

single-sided bolted connection. J Constr Steel Res 2013; 86(7): 153-166.

[46] CSA-S16-14. Design of steel structures. Toronto: Canadian Standards Association 2014.

[47] AS 4100-1998. Steel structures. Sydney, Australia: Australian Standard 1998.

[48] EN 1993-1-8:2005. Eurocode 3: design of steel structures - part 1-8: design of joints. Brussels, Belgium: European Committee for Standardization 2005.

[49] ANSI/AISC360-16. Specification for structural steel buildings. Chicago, IL, USA: American Institute of Steel Construction 2016.

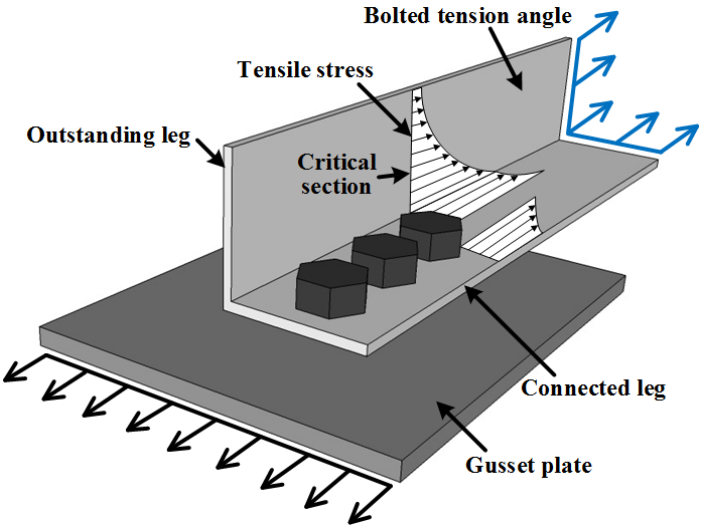

Fig. 1 Tensile stress distribution over the critical section of a bolted steel tension angle.

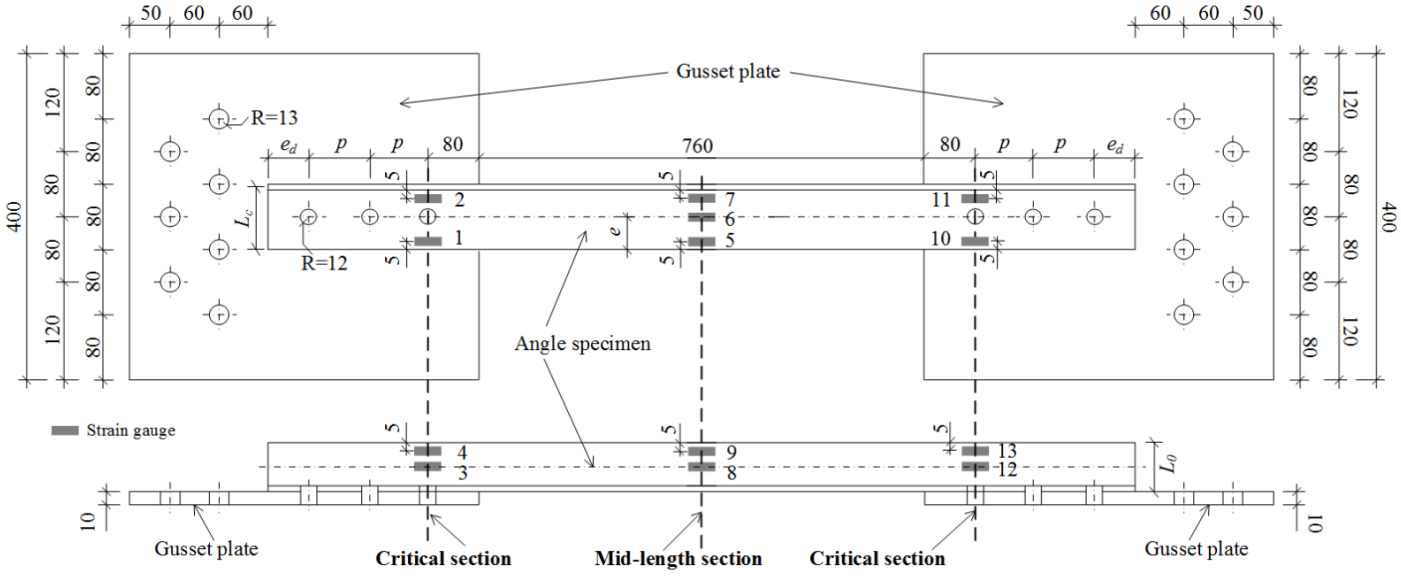

Fig. 2 Typical specimen configurations and instrumentations.

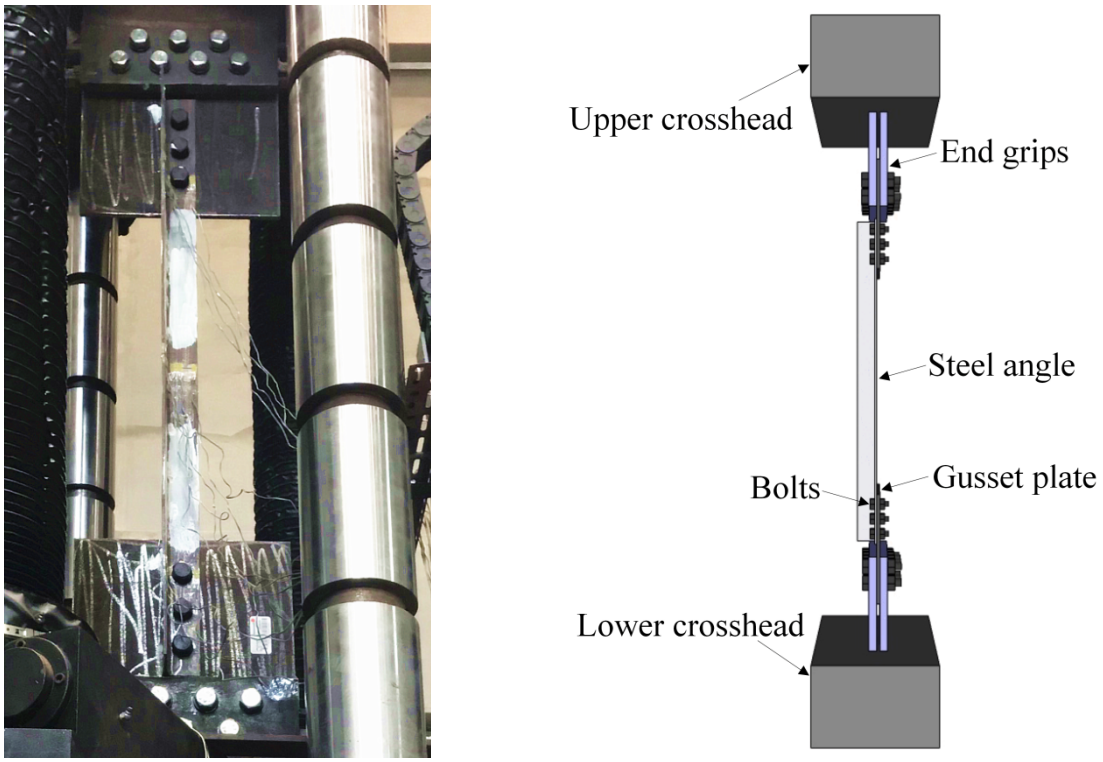

(a) (b)

Fig. 3 Test arrangement: (a) Front view and (b) Side view.

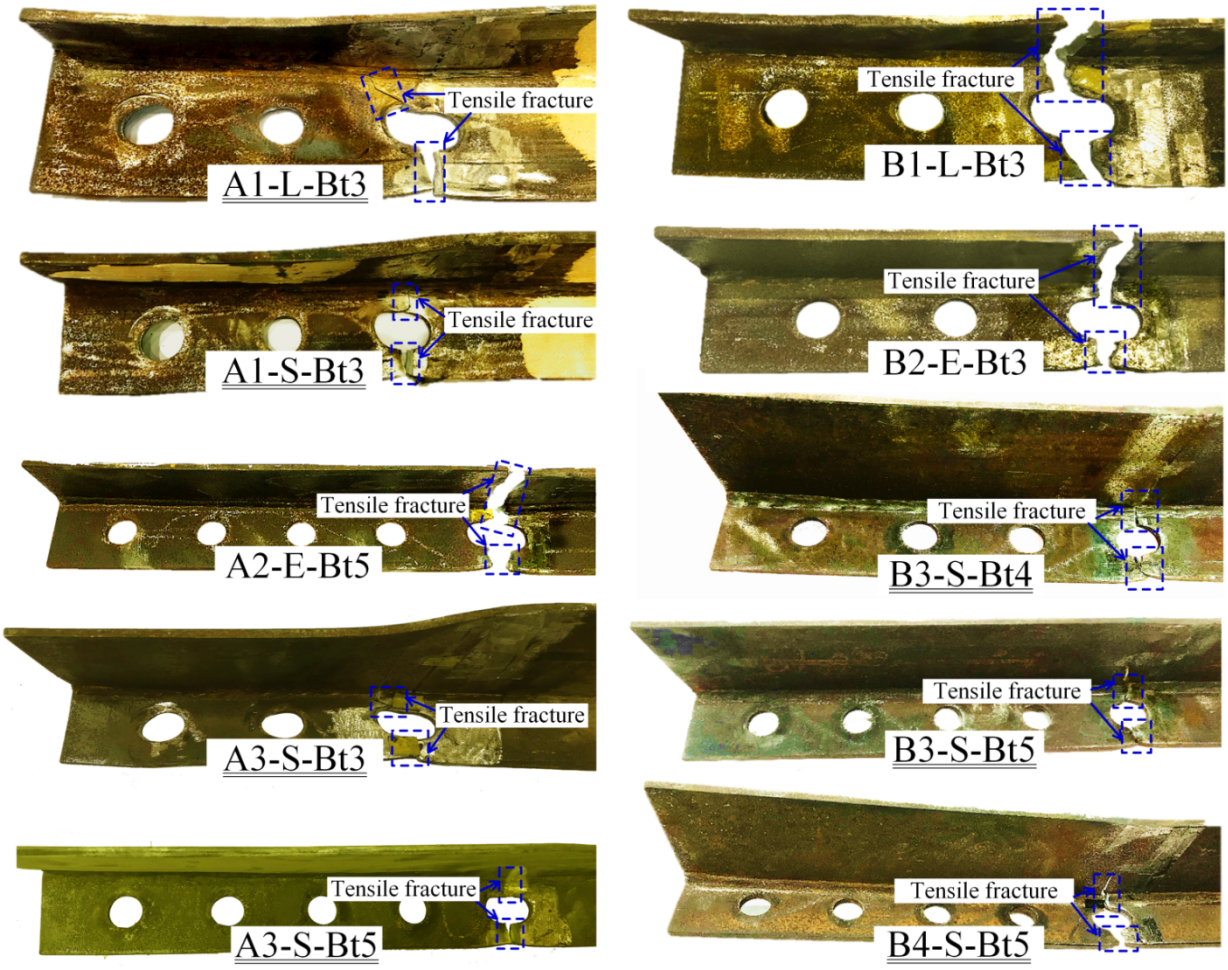

(a) (b)

Fig. 4 Typical failure modes of tension angles: (a) S275 angles and (b) S690 angles.

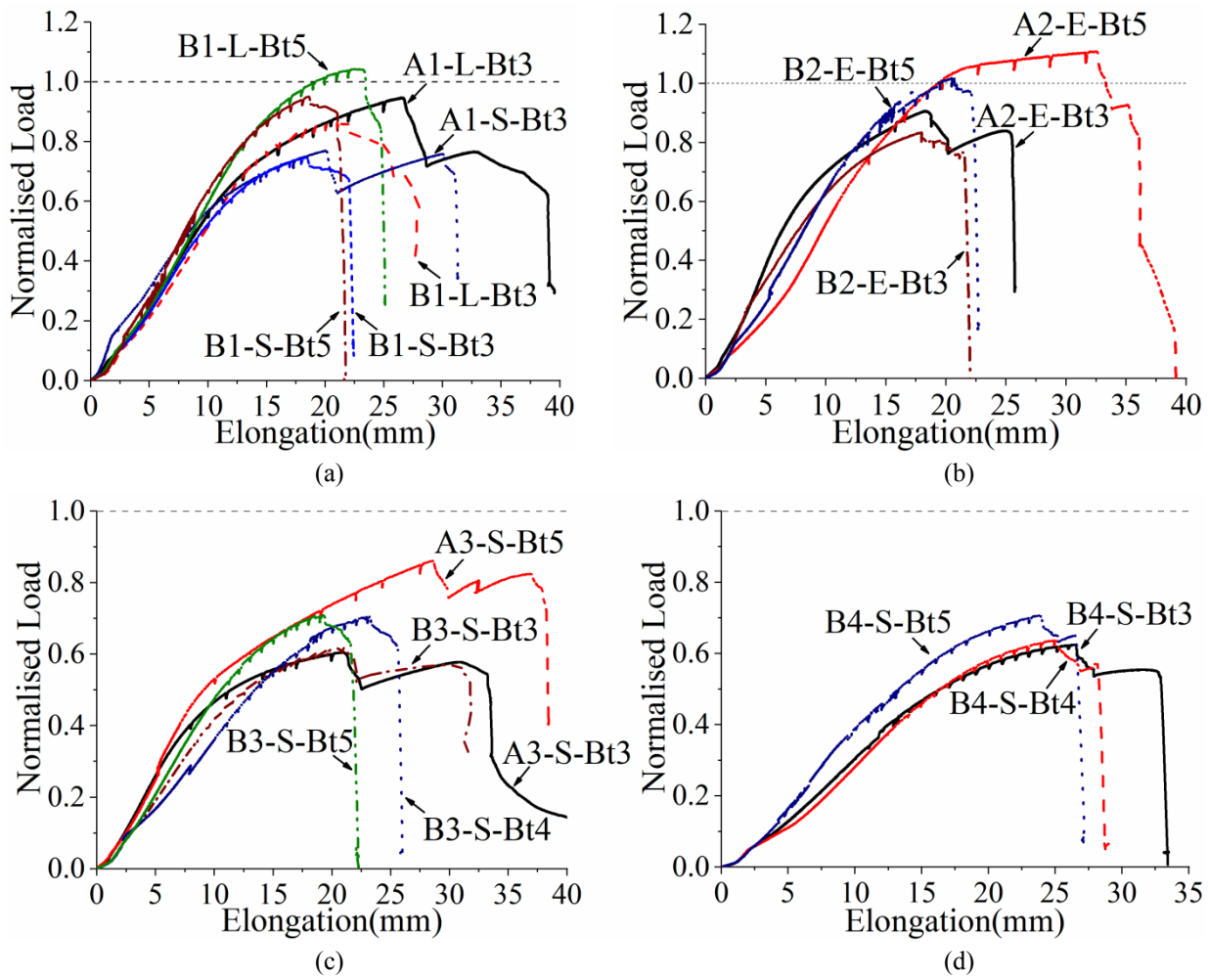

Fig. 5 Normalised load versus elongation curves: (a) A1/B1 series, (b) A2/B2 series, (c) A3/B3 series and (d) B4 series.

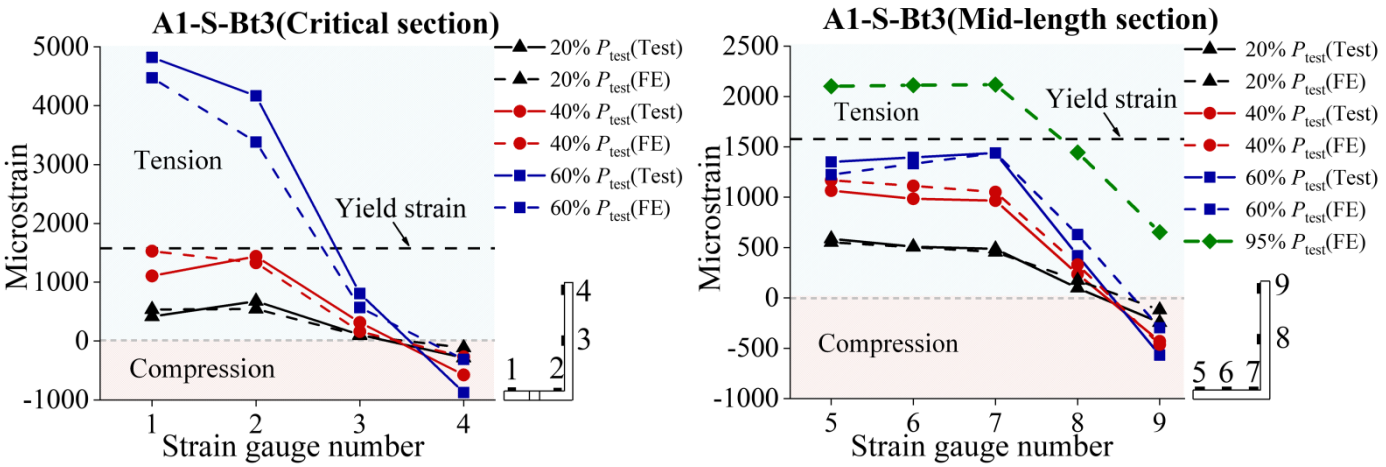
A1-S-Bt3(Critical section)
A1-S-Bt3(Mid-length section)
Microstrain
Strain gauge number
Tension
Compression
Yield strain
20% P_{test}(Test)
20% P_{test}(FE)
40% P_{test}(Test)
40% P_{test}(FE)
60% P_{test}(Test)
60% P_{test}(FE)
95% P_{test}(FE)

(a)

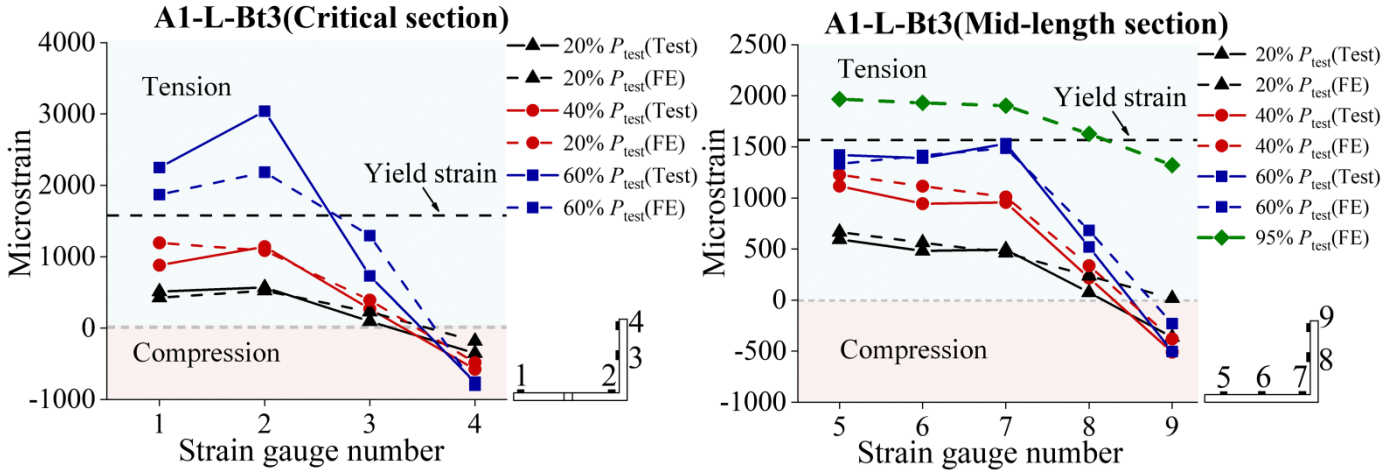
A1-L-Bt3(Critical section)
A1-L-Bt3(Mid-length section)
Microstrain
Strain gauge number
Tension
Compression
Yield strain
20% P_{test}(Test)
20% P_{test}(FE)
40% P_{test}(Test)
40% P_{test}(FE)
60% P_{test}(Test)
60% P_{test}(FE)
95% P_{test}(FE)

(b)

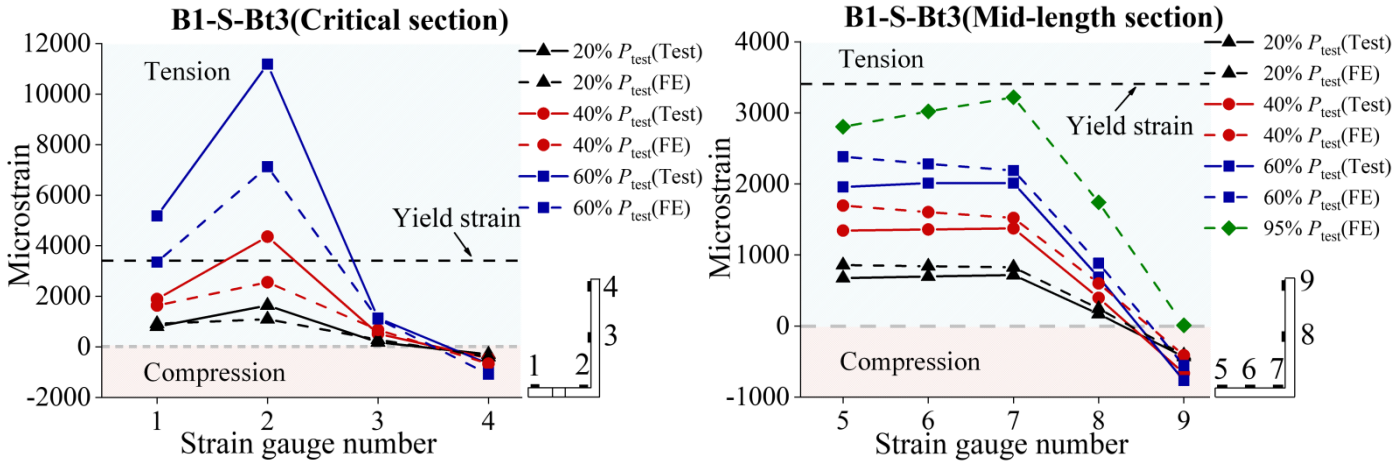
B1-S-Bt3(Critical section)
B1-S-Bt3(Mid-length section)
Microstrain
Strain gauge number
Tension
Compression
Yield strain
20% P_{test}(Test)
20% P_{test}(FE)
40% P_{test}(Test)
40% P_{test}(FE)
60% P_{test}(Test)
60% P_{test}(FE)
95% P_{test}(FE)

(c)

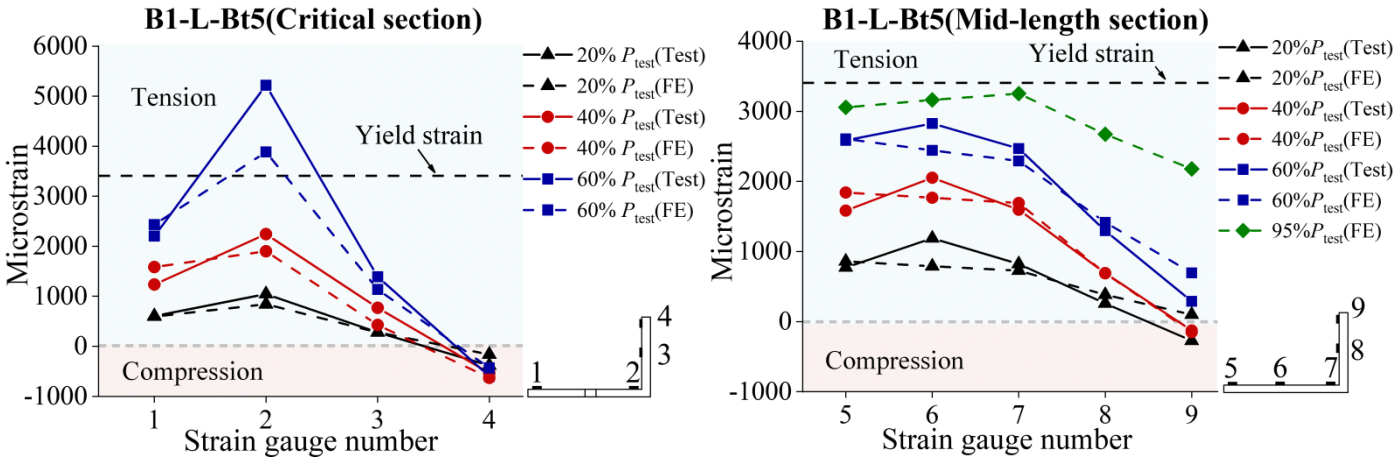

(d)

Fig. 6 Representative strain distributions: (a) A1-S-Bt3, (b) A1-L-Bt3, (c) B1-S-Bt3 and (d) B1-L-Bt5.

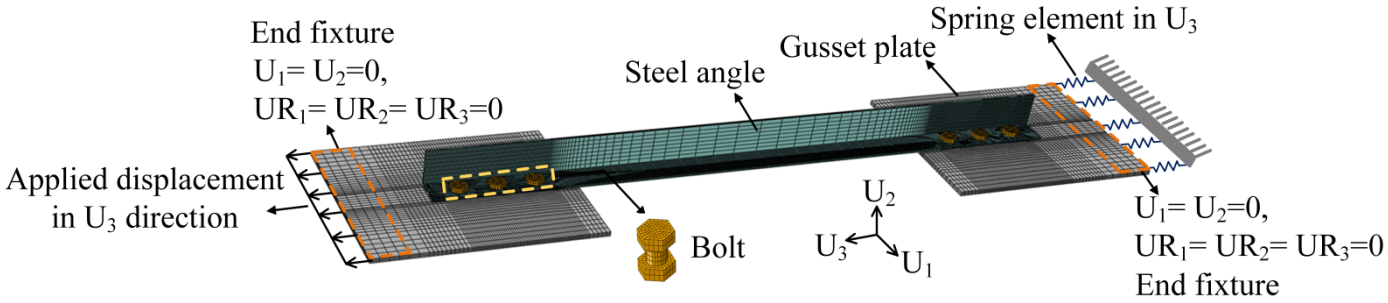

Fig. 7 Overview of finite element (FE) model.

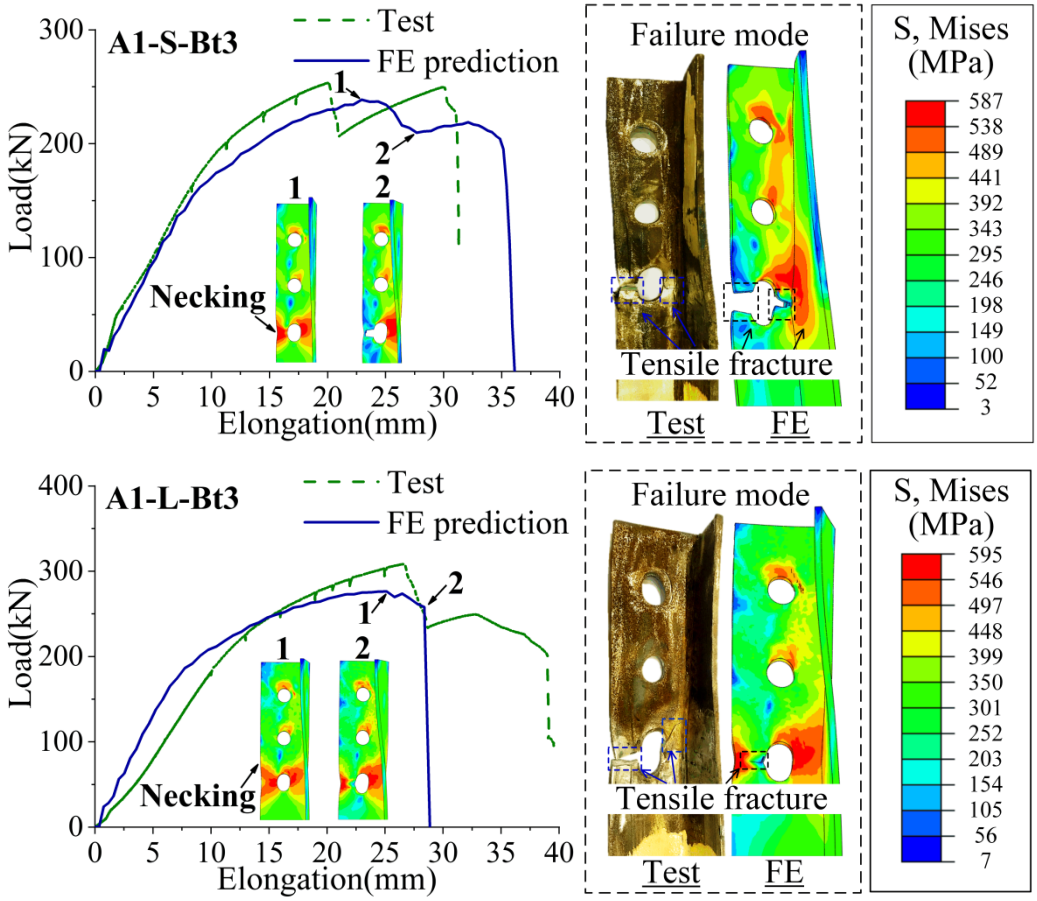

(a)

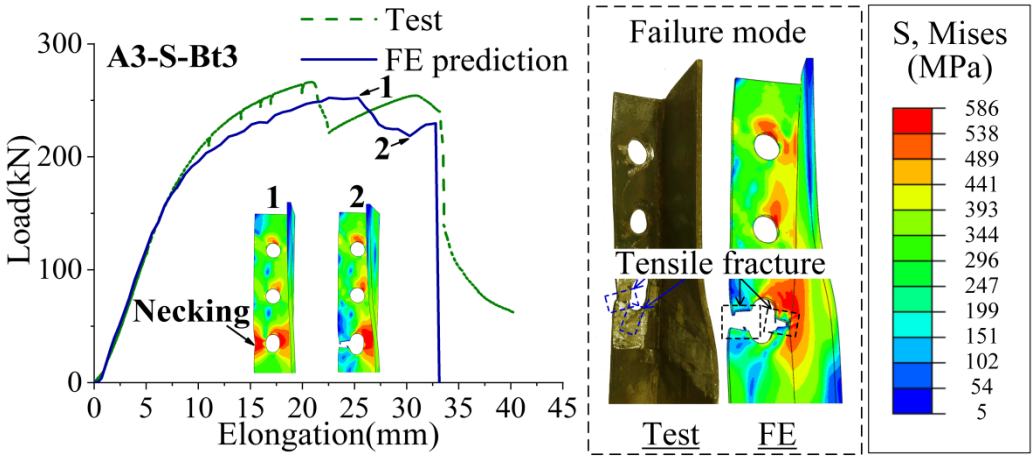
A3-S-Bt3
Test
FE prediction
Load(kN)
Elongation(mm)
Necking
1
2
Failure mode
Tensile fracture
Test
FE
S, Mises
(MPa)
586
538
489
441
393
344
296
247
199
151
102
54
5

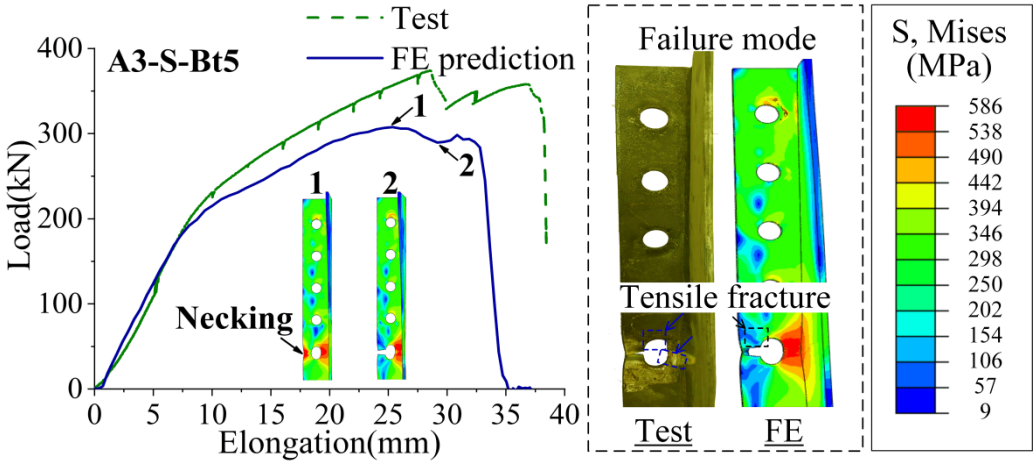
A3-S-Bt5
Test
FE prediction
Load(kN)
Elongation(mm)
Necking
1
2
Failure mode
Tensile fracture
Test
FE
S, Mises
(MPa)
586
538
490
442
394
346
298
250
202
154
106
57
9

(b)

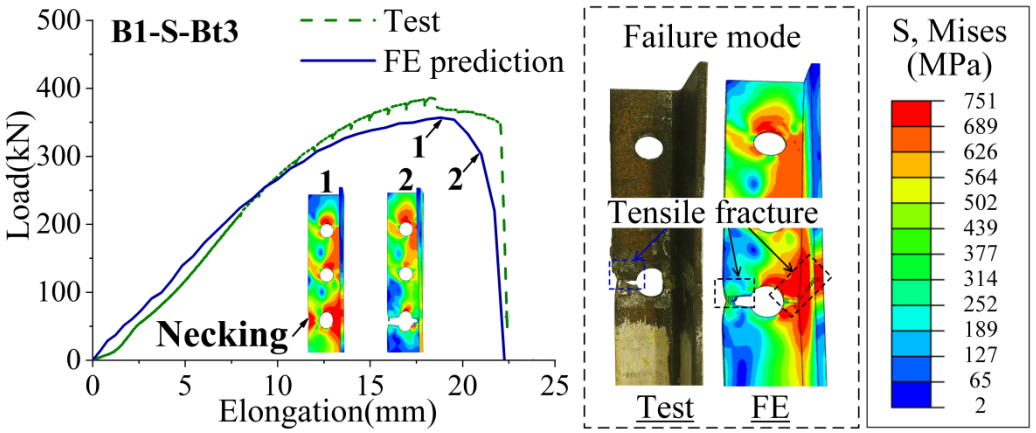
B1-S-Bt3
Test
FE prediction
Load(kN)
Elongation(mm)
Necking
1
2
Failure mode
Tensile fracture
Test
FE
S, Mises
(MPa)
751
689
626
564
502
439
377
314
252
189
127
65
2

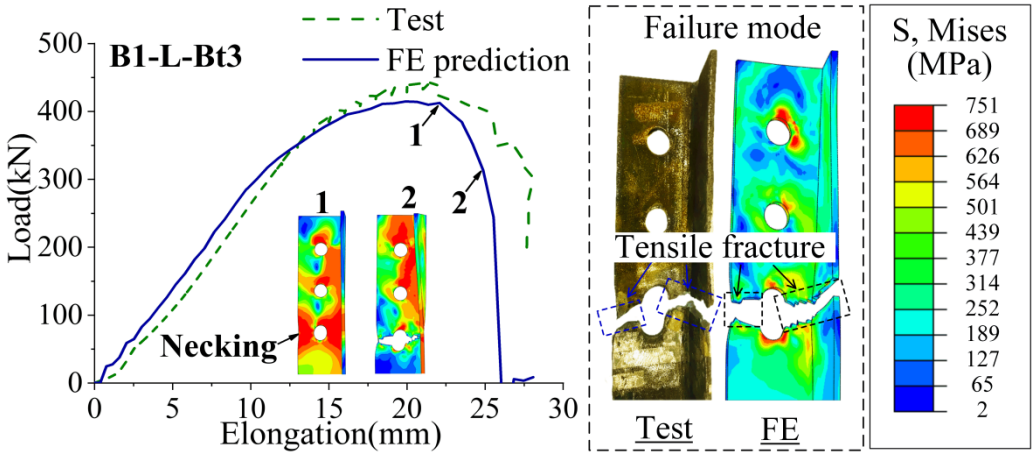
B1-L-Bt3
Test
FE prediction
Load(kN)
Elongation(mm)
Necking
1
2
Failure mode
Tensile fracture
Test
FE
S, Mises
(MPa)
751
689
626
564
501
439
377
314
252
189
127
65
2

(c)

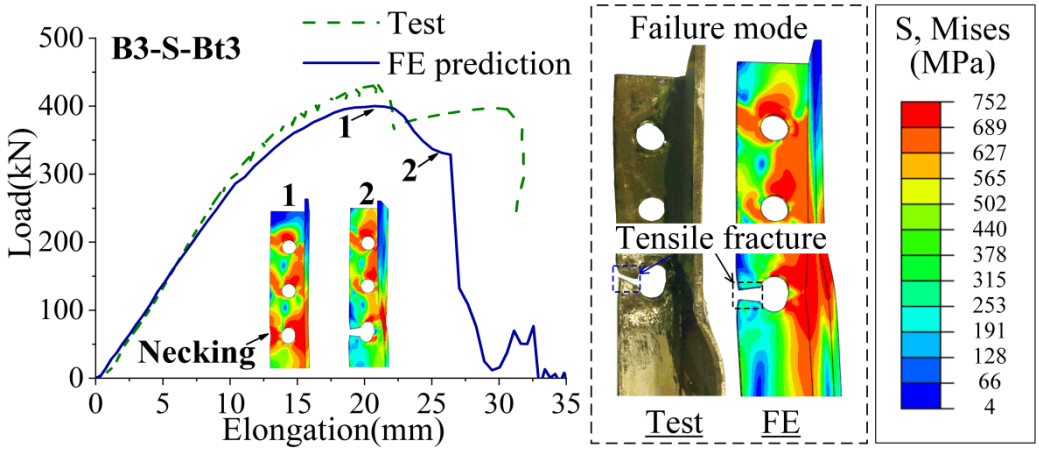

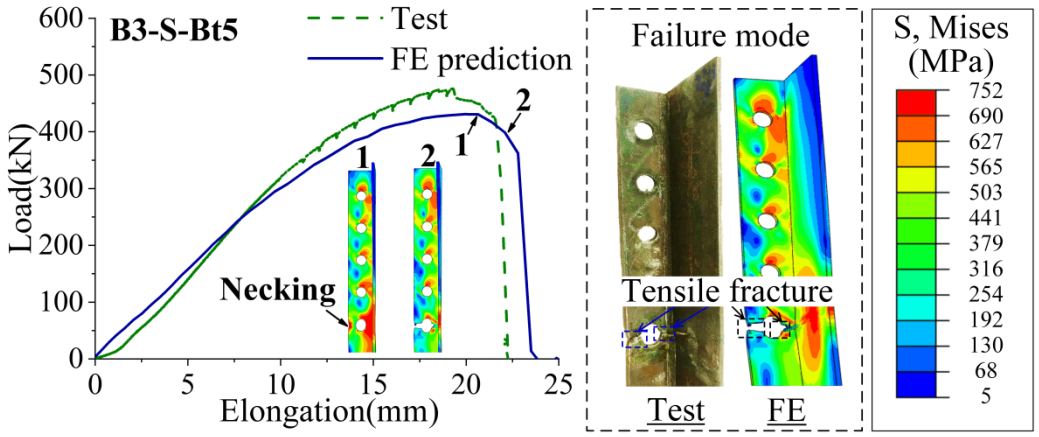

(d)

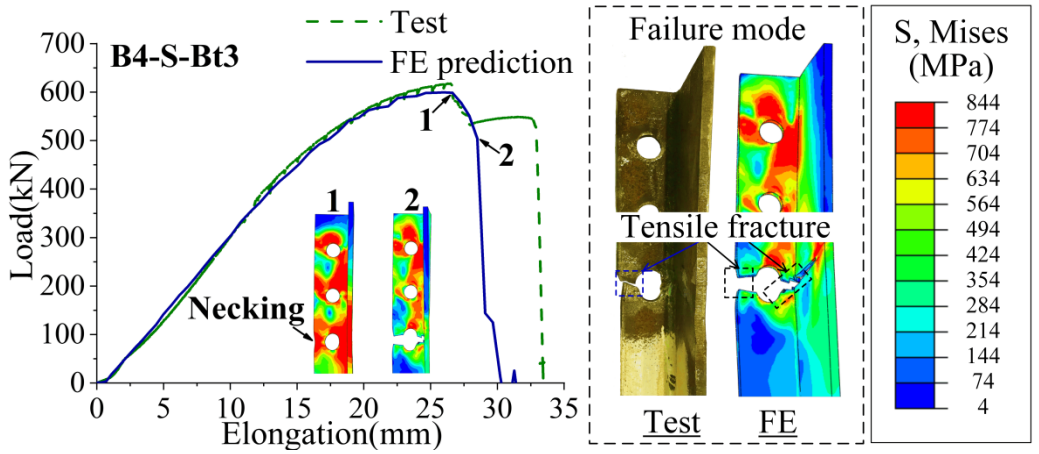

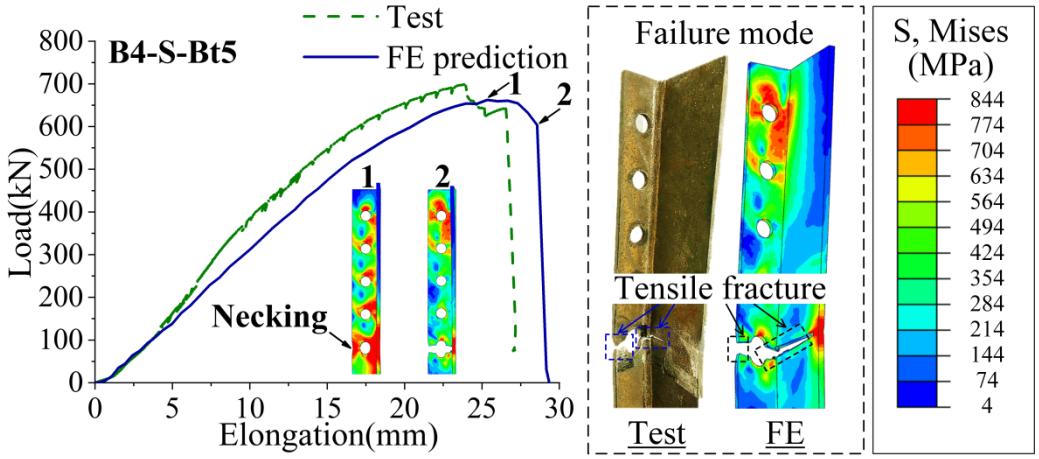

(e)

Fig. 8 Typical comparisons between test results and FE predictions: (a) A1 series, (b) A3 series, (c) B1 series, (d) B3 series and (e) B4 series.

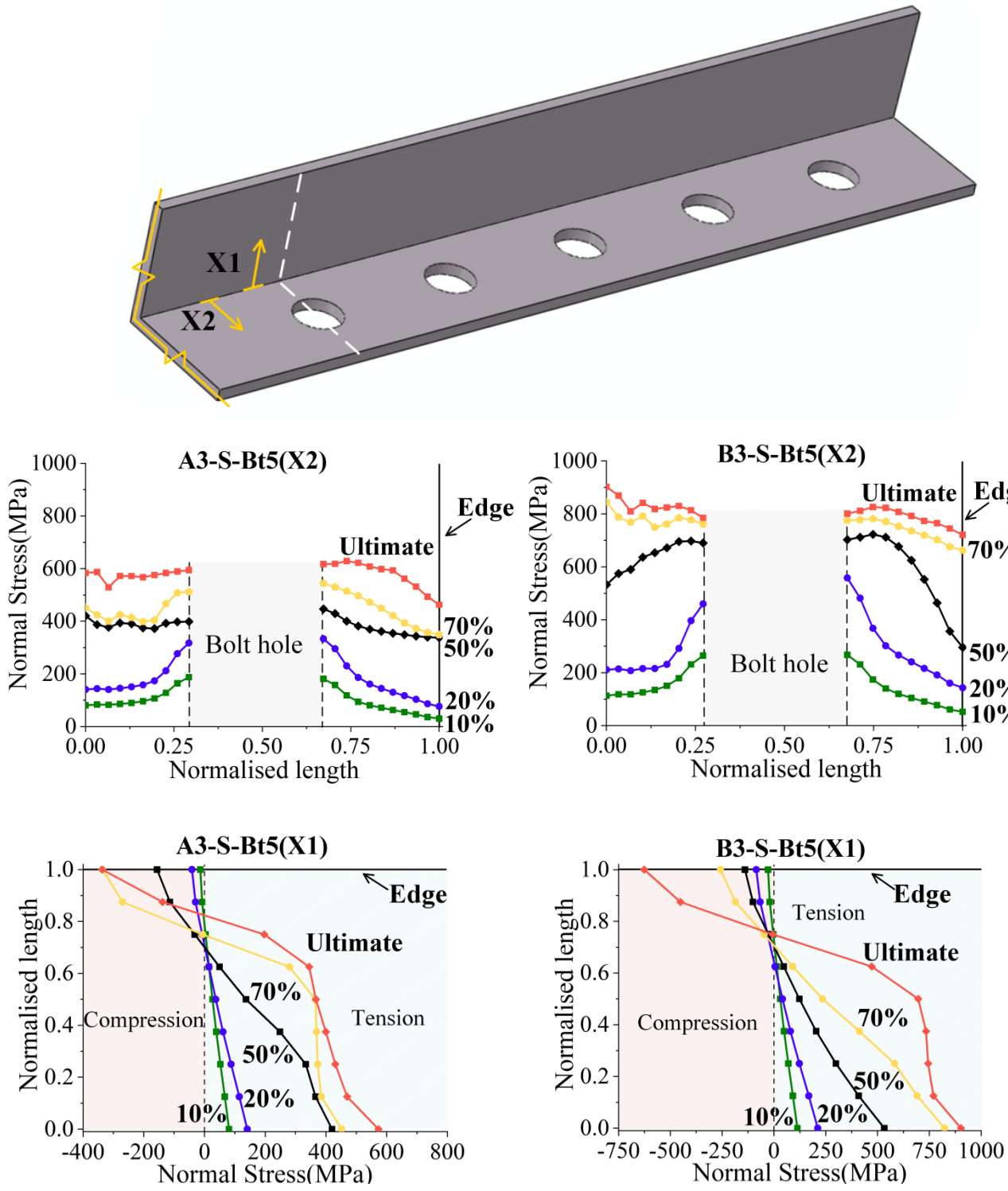

Fig. 9 Normal stress evolution at critical section of typical models.

Table 1 Specimen configurations, test resistance and predictions by finite element models

Specimen	*Dimension (mm)	Steel grade	Bolt No.	L_c (mm)	L_o (mm)	t (mm)	p (mm)	e_d (mm)	e (mm)	P_{test} (kN)	P_{norm}	P_{test}/P_{FE}
A1-L-Bt3	85×65×6	S275	3	86.0	63.0	5.75	74.86	57.97	41.61	297	0.92	1.08
A1-S-Bt3	85×65×6	S275	3	67.0	85.0	5.75	75.80	59.70	31.05	246	0.74	1.03
A2-E-Bt3	65×65×6	S275	3	67.0	68.0	5.75	74.66	58.54	31.43	250	0.88	1.05
A2-E-Bt5	65×65×6	S275	5	65.0	65.0	5.75	74.68	58.40	32.67	291	1.07	1.17
A3-S-Bt3	125×65×6	S275	3	65.0	125.5	5.75	74.71	59.01	31.29	258	0.59	1.02
A3-S-Bt5	125×65×6	S275	5	68.0	123.0	5.75	75.23	58.88	32.22	364	0.83	1.18
											Mean	1.09
											CoV	0.065
B1-L-Bt3	85×65×6	S690	3	85.0	63.0	5.94	75.05	59.83	41.14	432	0.85	1.04
B1-L-Bt5	85×65×6	S690	5	84.0	65.0	5.94	74.97	60.14	43.27	516	1.01	1.10
B1-S-Bt3	85×65×6	S690	3	63.0	85.0	5.94	75.89	61.37	32.20	377	0.74	1.06
B1-S-Bt5	85×65×6	S690	5	65.0	84.0	5.94	74.91	59.65	32.87	470	0.92	1.12
B2-E-Bt3	65×65×6	S690	3	66.0	66.0	5.94	75.18	60.28	31.82	352	0.80	1.01
B2-E-Bt5	65×65×6	S690	5	66.0	64.0	5.94	74.68	59.47	31.75	421	0.98	1.11
B3-S-Bt3	125×65×6	S690	3	66.0	125.0	5.94	74.97	60.53	32.00	421	0.61	1.05
B3-S-Bt4	125×65×6	S690	4	65.0	123.0	5.94	74.53	59.95	32.18	469	0.69	1.12
B3-S-Bt5	125×65×6	S690	5	64.5	122.0	5.94	75.02	58.68	30.82	465	0.69	1.08
B4-S-Bt3	125×65×8	S690	3	65.0	125.0	7.88	76.00	59.80	31.43	605	0.61	1.01
B4-S-Bt4	125×65×8	S690	4	64.0	125.0	7.88	75.06	59.43	31.74	626	0.63	1.01
B4-S-Bt5	125×65×8	S690	5	65.0	125.5	7.88	74.91	59.75	31.04	685	0.68	1.03
											Mean	1.06
											CoV	0.041

*The connected leg is underlined.

Table 2 Material properties

Material	Elastic modulus (GPa)	Yield stress f_y (MPa)	Tensile strength f_u (MPa)	Ultimate strain ε_u	f_u/f_y
S690 angle plate (6 mm)	185	640	715	0.061	1.12
S690 angle plate (8 mm)	200	770	800	0.060	1.04
S690 gusset plate (gusset plate)	195	705	730	0.060	1.04
S275 angle plate	195	310	470	0.163	1.52

Table 3 Design equations for net section resistance of tension members

References	Design equations
CSA S16-14 [46]	$P_{CSA}= \psi A_e f_u$ where P_{CSA} is the design rupture resistance for a tension member; ψ is the resistance factor; f_u is the ultimate tensile strength of steel and A_e is the effective area considered for shear lag. For angles connected by only one leg with four or more transverse lines of fasteners, A_e=0.80A_n, where A_n is the net area. In cases with fewer than four transverse lines of fasteners, A_e=0.60A_n.
AS4100-1998 [47]	The design resistance of a tension member is expressed as: $P_{AS}= \psi 0.85 k_t A_n f_u$ where ψ is the capacity factor; k_t is the correction factor for distribution of forces (i.e. shear lag effects), taken as 0.85 for equal leg angles and unequal leg angles connected by the long leg, or 0.75 for unequal leg angles connected by the short leg, or 0.9 for tee members; A_n is the net area of the cross-section, obtained by deducting from the gross area the sectional area of all penetrations and holes, including fastener holes and f_u is the ultimate tensile strength.
Eurocode3 Part 1-8 [48]	A single angle in tension connected by a single row of bolts in one leg may be treated as concentrically loaded over an effective net section for which the design ultimate resistance should be determined as follows: 1) with 1 bolt: $P_{EC3=}\dfrac{2.0(e_2 - 0.5d_0)tf_u}{\gamma_{M2}}$ 2) with 2 bolts: $P_{EC3=}\dfrac{\beta_2 A_n f_u}{\gamma_{M2}}$ 3) with 3 or more bolts: $P_{EC3=}\dfrac{\beta_3 A_n f_u}{\gamma_{M2}}$ where β_2 and β_3 are reduction factors dependent on the pitch and A_n is the net area of the angle. For an unequal-leg angle connected by its short leg, A_n should be taken as equal to the net section of an equivalent equal-leg angle of leg size equal to that of the short leg; f_u is the ultimate tensile strength of the steel and γ_{M2} is the partial safety factors for resistance of bolts.
AISC 360-16 [49]	$P_{AISC} =\psi A_e f_u$ where P_{AISC} is the nominal axial strength; ψ is the resistance factor for tension rupture; f_u is the ultimate tensile strength of steel and A_e is the effective area of the member cross-section. For members with bolted connections, it is obtained from $A_e=UA_n$ where A_n is the net area of a member (i.e. the sum of the products of the thickness and the net width of each element) and U is the reduction coefficient, as given by $U=1-\bar{x}/l$ where $\bar{x}$ is the eccentricity of the connection and l is the connection length.

Table 4 Performance of design equations

Specimen	P_{test}/P_{AISC}	P_{test}/P_{EC3}	P_{test}/P_{CSA}	P_{test}/P_{AS}	P_{test}/P_{Yam}
A1-L-Bt3	1.03	1.66	1.53	1.27	0.90
A1-S-Bt3	0.90	1.57	1.24	1.17	0.97
A2-E-Bt3	1.01	1.58	1.46	1.21	1.00
A2-E-Bt5	1.14	1.94	1.34	1.48	1.13
A3-S-Bt3	0.84	1.72	0.99	0.93	1.01
A3-S-Bt5	0.97	2.29	1.04	1.31	1.15
Mean	0.98	1.79	1.27	1.23	1.03
CoV	0.108	0.154	0.173	0.148	0.095
B1-L-Bt3	0.95	1.54	1.42	1.18	0.92
B1-L-Bt5	1.07	1.82	1.26	1.40	1.05
B1-S-Bt3	0.91	1.67	1.25	1.18	1.09
B1-S-Bt5	1.01	1.98	1.15	1.44	1.19
B2-E-Bt3	0.92	1.45	1.34	1.11	0.99
B2-E-Bt5	1.04	1.78	1.22	1.36	1.12
B3-S-Bt3	0.86	1.73	1.01	0.96	1.12
B3-S-Bt4	0.85	1.96	0.86	1.08	1.12
B3-S-Bt5	0.81	1.98	0.87	1.09	1.05
B4-S-Bt3	0.86	1.76	1.01	0.95	1.16
B4-S-Bt4	0.78	1.84	0.79	0.99	1.07
B4-S-Bt5	0.80	2.00	0.86	1.07	1.09
*P-A1-60L	0.96	1.79	1.12	1.24	0.95
*P-A1-75L	1.00	1.72	1.19	1.31	1.00
*P-A1-90L	0.99	1.58	1.18	1.31	0.98
*P-A1-75S	0.86	1.74	0.99	1.24	1.05
*P-A2-60S	0.82	1.95	0.88	1.10	1.05
*P-A2-75S	0.82	1.80	0.91	1.14	1.04
*P-A2-90S	0.81	1.68	0.92	1.16	1.04
Mean	0.90	1.78	1.06	1.17	1.06
CoV	0.100	0.087	0.175	0.122	0.065

*Specimens P-A1-60L, P-A1-75L, P-A1-90L, P-A1-75S, P-A2-60S, P-A2-75S and P-A2-90S refer to A1-60L, A1-75L, A1-90L, A1-75S, A2-60S, A2-75S and A2-90S in the previous test programme conducted by the authors and colleagues [32].

Declaration of interests

The authors declare that they have no known competing financial interests or personal relationships that could have appeared to influence the work reported in this paper.

Author statement

Michael CH Yam: Conceptualization, Methodology, Writing-Reviewing and Editing, Supervision, Funding acquisition
Ke Ke*: Writing- Original draft preparation, Writing-Reviewing and Editing, Software, Validation, Formal analysis,
Binhui Jiang: Investigation, Visualization
Angus CC Lam: Investigation, Resources, Project administration